PCCP

Accepted Manuscript

ROYAL SOCIETY OF CHEMISTRY

www.rsc.org/pccp

Graphene quantum dots boost the capacitance of the graphene supercapacitor more than 90% and with an excellent long-term stability.

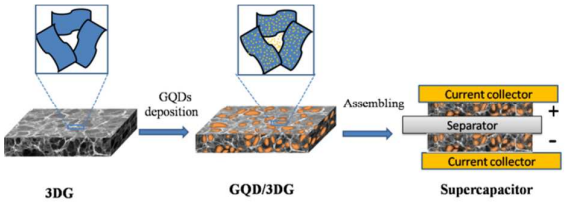

Cite this: DOI: 10.1039/c0xx00000x

www.rsc.org/xxxxxx

ARTICLE TYPE

Graphene Quantum Dots/Three-Dimensional Graphene Composites for High-Performance Supercapacitors

Qing Chen,‡ Yue Hu,‡ Chuangang Hu, Huhu Cheng, Zhipan Zhang,* Huibo Shao and Liangti Qu*

Received (in XXX, XXX) Xth XXXXXXXXX 20XX, Accepted Xth XXXXXXXXX 20XX

DOI: 10.1039/b000000x

Graphene quantum dots (GQDs) have been successfully deposited onto the three-dimensional graphene (3DG) by a benign electrochemical method and the ordered 3DG structure remains intact after the uniform deposition of GQDs. In addition, the capacitive properties of the as-formed GQD/3DG composites are evaluated in symmetrical supercapacitors. It is found that the supercapacitor fabricated from the GQD/3DG composite is highly stable and exhibits a high specific capacitance of 268 F g^{-1}, representing a more than 90% improvement over that of the supercapacitor made from pure 3DG electrodes (136 F g^{-1}). Owing the convenience of the current method, it can be further used in other well-defined electrode materials, such as carbon nanotubes, carbon aerogels and conjugated polymers to improve the performance of the supercapacitors.

Introduction

With the fast-increasing demands for mini-sized energy storage devices in portable electronics, power backups, electrical vehicles and various micro-power systems, supercapacitors have been attracting more and more interests from researchers in different fields owing to their fast charge-discharge rates and long lifetimes.[1–3] Supercapacitors, also known as electrochemical capacitors (ECs), can be classified into two types according to their energy storage mechanisms, the electrochemical double layer capacitors (EDLCs) that store energy at the electrode/electrolyte interface [4,5] and pseudo-capacitors that involve fast and reversible faradaic reactions of electro-active species including conjugated polymers [6] and various transition metal oxides such as RuO_2,[7] Co_3O_4,[8] MnO_2,[9,10] $Ni(OH)_2$,[11] etc. Despite of the great efforts paid to the synthesis of carbon-based electrode materials, a facile synthesis of carbon materials with large surface area, high conductivity, and suitable pore size distribution for high performance supercapacitor applications still remains elusive and is therefore of great practical interest and importance.

The electrode material is the key component determining the capacitance performance of EDLCs. Carbonaceous materials, such as activated carbons, carbon nanotubes and graphene,[6,12] have been selected to work as electrochemical double layer (EDL) active materials to fabricate supercapacitors, owing to their large specific surface area, low fabrication cost, abundant resource and satisfactory electrochemical stability. However, most materials usually have uncontrollable pore structures, extensive oxygenated functionalities and are thus of low conductivities, limiting their device performance.[13] To solve these problems, it would be desirable to develop highly ordered carbon materials with narrow pore size distributions, interconnected pore structures and short pore lengths in order to improve the specific capacitance and the response time of supercapacitors.

Graphene has been recognized as an attractive next-generation carbon material for fabricating high-performance supercapacitors due to its low mass density,[14] excellent electrical conductivity, and high specific surface area.[15–17] However, the direct application of graphene materials in supercapacitors has been hindered by graphene's nature to agglomerate. Due to the strong π-π interaction between the basal planes of graphene sheets, graphene-based electrodes prepared from uncontrolled assembling of graphene sheets are mainly composed of irregular aggregates and lack of sufficiently large pores to allow the facile access of electrolytes.[18] If one may assemble graphene platelets in a hierarchical way and obtain architectures with mesopores in the interconnected microporous scaffolds, ions in the electrolyte can easily diffuse to the interior surface for extensive EDL formation over larger accessible surfaces and potentially lead to more effective energy storage devices.[19] Recently, graphene structures with tunable macroscopic three-dimensional (3D) porous networks have emerged as a promising paradigm for electrode materials used in energy conversion and storage devices.[20–22] The 3D graphene (3DG) macrostructures generally feature an interconnected network with mesopores in nanometers and ordered channels in micrometers, enabling the easy access and diffusion of ions and molecules throughout the highly porous structures. Apart from the high porosity and large specific surface area, these graphene materials are further of strong mechanical properties and fast electron transport kinetics due to the combination of the 3D porous structure and the excellent intrinsic electric properties of graphene.[23] Therefore, it would be interesting to study the modification and application of the 3DG structure as a versatile platform to improve the performance of

different energy-related devices. Particularly for supercapacitors, as the specific capacitance of an EDLC comes from the charge accumulation at the electrode/electrolyte interface that is mainly dependent on the pore structure of the electrode and accessible surface area to the electrolyte, 3DG network could serve as the basic scaffold to assemble other electrochemically active materials to boost the overall capacitance of the EDLCs.

Graphene quantum dots (GQDs) are the new type of quantum dots (QDs), which are single- or few-layer graphenes with a tiny size of only several nanometers and have unique properties both of graphene and QDs due to the pronounced quantum confinement and edge effects.[24] Owing to their desiring advantages of high electron mobility, tunable band gaps, good bio-compatibility and excellent dispersability in various solvents,[25,26] GQDs have been studied in the design and fabrication of novel devices in multidisciplinary fields such as bio-imaging,[27] bio-sensing,[28] photovoltaics,[29] fuel cells [17] and light-emitting diodes.[30] Very recently, the electrochemical capacitive properties of GQDs and their applications in GQDs micro-supercapacitors,[31] CQD/RuO_2 supercapacitors [32] and GQDs-CNTs supercapacitors [33] have shown that GQDs can considerably improve the performance of supercapacitors. Considering the advantages of the 3DG and GQDs, it is reasonable to expect that a novel composite of 3DG and GQDs would be an ideal electrode material for fabricating high-performance supercapacitor to their counterparts of 3DG or GQDs, as the deposition of GQDs on the 3DG scaffold would improve the specific surface area of the 3DG electrode and create additional micropores that would significantly contribute to the overall electrochemical capacitance due to the tiny size of the GQDs.

Herein we report a high-performance supercapacitor based on a new composite with hierarchically porosity based on GQDs decorated on 3DG slices as the building scaffolds. The as-formed GQD/3DG slices were homogeneous in structure and the symmetrical supercapacitors fabricated with the GQD/3DG electrodes showed a significantly enhanced specific electrochemical capacitance of 268 F g^{-1}, standing for a more than 90% performance increase compared to that of its counterpart with pristine 3DG electrodes (136 F g^{-1}).

Experimental

Preparation of GQDs

GQDs used in this work were prepared by an electrochemical method similar to our previous report.[24] Briefly, a carbon rod was selected as the working electrode and scanned for several hundred cycles by cyclic voltammetry (CV) within ±3 V at scan rate of 0.5 V s^{-1} in 0.1 M phosphate buffer solution (PBS). The Ag/AgCl electrode and a Pt wire were used as the reference electrode and the counter-electrode, respectively. After several cycles of CV scanning, the original PBS solution turned to yellow due to the formation of the GQDs. With an increasing number of scanning cycles, the color of the PBS solution further changed to dark yellow and even black. The as-produced water-soluble GQDs were purified by filtering and dialyzing with the cellulose ester membrane bag (MD77, 800-1400) for several days to fully remove the supporting electrolyte of PBS.

Preparation of 3DG and GQD/3DG composite

3DG was prepared by heating 2 mg mL^{-1} of homogeneous graphene oxide (GO) aqueous dispersion sealed in a Teflon-lined autoclave at 180 °C for 12 h. A part of the obtained 3DG was transferred onto a microscope slide, gently pressed to a thin film with another glass slide, and then cut the film into two identical squares of the same size (*ca.* 0.2 cm × 0.2 cm) with a knife. As shown in Scheme 1, the two square 3DG electrodes were separated by a piece of filter paper soaked with 1 M H_2SO_4 electrolyte and thus assembled in a symmetrical two-electrode configuration with gold flakes of 0.3 cm × 0.5 cm as the current collector to give Device A. To prepare the GQD/3DG composite, the 3DG with the same size to that mentioned above was used as the working electrode and pretreated by cyclic voltammetry (CV) scans to make them more hydrophilic in order to enhance the reactivity with the aqueous GQDs solution. The 3DG electrode was then immersed in the purified GQDs solution and GQDs were subsequently electrodeposited on the surface of the 3DG by applying a bias at +2 V for 5 h and 10 h in a three-electrode system to give GQD/3DG composite samples of GQD/3DG-5h and GQD/3DG-10h, respectively. The change in the mass of the 3DG is between 1.4 to 5% after 10 h GQD deposition (Table S1) and thus deemed to only slightly influence the calculation of mass-specific capacitance of the electrode. The as-synthesized GQD/3DG composite electrodes were assembled in the same symmetrical two-electrode configuration to give Device B (5 h GQD deposition), C (10 h GQD deposition) directly without using a binding agent and/or conducting additive, respectively. To exclude any significant capacitance improvement due to the GQD deposition process, control samples of 3DG was immersed in a *GQD-free* solution and subjected to a +2 V bias for 10 h before they were eventually assembled in the same two-electrode configuration as Device D.

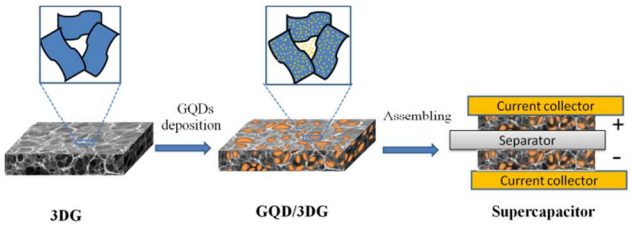

Scheme 1. Cartoonic representation of fabricating a symmetrical supercapacitor based on the GQD/3DG composite material. 3DG was first prepared by one-step hydrothermal method before the deposition of GQDs and the supercapacitor was assembled by separating two GQD/3DG electrodes with a piece of filter paper soaked with the 1 M H_2SO_4 electrolyte.

Characterization

The morphology of the samples was explored by scanning electron microscopy (SEM, JSM-7500F) and transmission electron microscopy (TEM, 7650B, Hitachi) techniques. Raman spectra were recorded by using a RM 2000 microscopic confocal Raman spectrometer (Renishaw PLC, England) with a 514 nm laser as the excitation source. The X-ray diffraction (XRD) was carried by D8 advance of Brooks. The electrical resistance was measured by using Keithley 4200-SCS semiconductor

characterization system. Nitrogen sorption measurements were carried out with a Quantachrome Autosorb-IQ gas adsorption analyzer at 77 K. The CV and galvanostatic charge/discharge curves were measured between 0 and 0.8 V and the electrochemical impedance spectra (EIS) were taken at the open-circuit potential in the frequency range of 0.01-10^5 Hz with a modulating amplitude of 5 mV.

Results and Discussion

Structure and morphology

High-quality 3DG was selected as the skeleton for the deposition of GQDs and its representative side-view is shown in Fig. 1a. The 3DG cylinder was about 2 cm in height and 1.3 cm in diameter. The GQD/3DG composite was then prepared by immersing the 3DG in a solution of GQDs and electrodepositing the GQDs on the 3DG electrode. As shown in Fig. 1b, no noticeable change in visual appearance was found after the deposition of GQDs, showing that the 3DG is a good platform for the controlled anchorage of GQDs. To assemble and measure the performance of the symmetrical supercapacitor, we cut the GQD/3DG block into squares of approximately 0.2 cm×0.2 cm in size (Fig. 1c). The microstructure of (a) to (c) was characterized by the scanning electron microscopy (SEM) and typical SEM images are shown in Fig. 1d to 1e. The original 3DG used in this study was freeze-dried and formed by physical cross-linking of graphene sheets, and as shown in Fig. 1d, 3DG clearly featured with the macropores in sizes ranging from submicrometer to several micrometers, a unique structure enabling the GQD solution to easily penetrate through the 3DG and having GQDs electrodeposited thereon. Following the assembling of GQDs on the surface of 3DG (Fig. 1e), the 3D structure remained intact, even after the GQD/3DG composite was cut into slices (Fig. 1f), suggesting the excellent mechanical properties of the 3DG and GQD/3DG electrodes. As the GQDs decorated on the 3DG surface were only about 2 to 5 nm in diameter, it is thus too small to be seen in the SEM images.

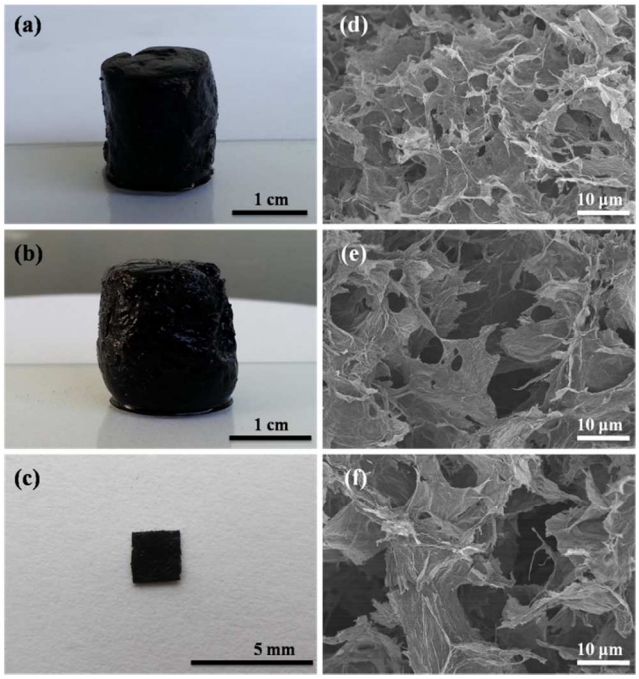

Fig. 1. Photographs of the 3DG (a), the GQD/3DG electrode with 10 h GQDs deposition (b) and the GQD/3DG slice for assembling the supercapacitor (c). (d), (e) and (f) are corresponding SEM images of (a), (b) and (c), respectively. The scale bars are 10 μm for (d), (e) and (f).

The transmission electron microscopy (TEM) was employed to confirm the anchorage of GQDs onto the surface of 3DG. As shown in Fig. 2a, the few-layer graphene sheets were almost transparent under TEM and the edge of the 3DG manifested itself by a multi-layered structure, suggesting the 3DG prepared by the direct hydrothermal method was formed by the stacking of multiple graphene layers. The as-synthesized GQDs (Fig. 2b and 2c) were mono-disperse with a uniform diameter of *ca*. 2–5 nm, in good accordance with our recent work. In contrast, the TEM image of GQD/3DG composite demonstrates that the GQDs formed a fairly blurry small dot-stacked structure on the surface of the 3DG and the GQDs could no longer be individually resolved (Fig. 2d), as was also observed in our recent work of assembling zero-dimensional GQDs into one-dimensional nanotubes with the aid of templates.[33] Although it is not accurate to determine the pore size by TEM, gaps less than 1 nm pores could be seen in the porous structure, implying the presence of micropores commensurate to few nm in the GQD/3DG composite. The enlarged view of the dots shown in the inset of Fig. 2d reveals the interplanar spacing of 0.334 nm, well corresponding to the interlayer distance of 0.34 nm between the (002) plane in the original GQDs (*vide infra*).[34,35]

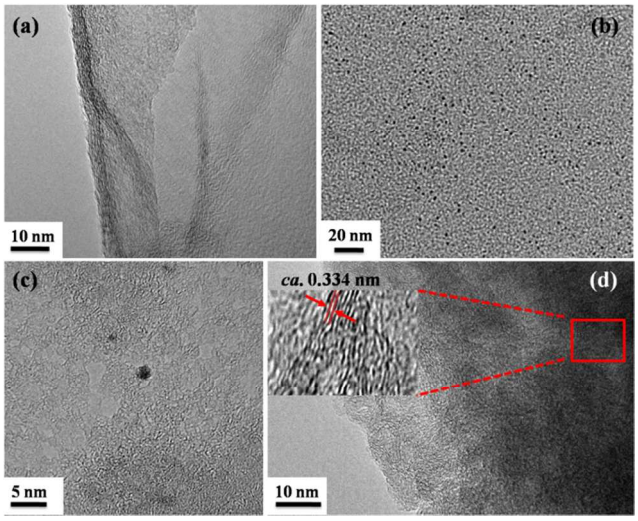

Fig. 2. TEM images of (a) the as-prepared 3DG, (b) GQDs, (c) a single GQD, and (d) GQD/3DG composite with 10 h GQDs deposition. The magnified view of the red area is shown as the inset of (d). Scale bars are 10 nm, 20 nm, 5 nm and 10 nm for a, b, c and d, respectively.

XRD and Raman spectroscopy were further used to characterize the GQD/3DG composite. As compared in Fig. 3a, the XRD patterns of 3DG and GQD/3DG exhibit a broad peak centered at 2θ of 24.6° and 24.9 °, respectively, corresponding to a similar interlayer spacing of 3DG and GQDs.[36,37] Raman spectra of graphene materials generally show characteristic peaks of "disorder" D-band and the crystalline G-band. The D and G bands originate from disorder band caused by the graphite edges and the in-phase vibration of the graphite lattice, respectively, and the relative intensity ratio of D-band and the G-band (I_D/I_G) is an indicator of the edge-quality of the carbon material. As plotted in Fig. 3b, Raman spectra of the 3DG and GQD/3DG composite of 10 h GQD deposition both show the characteristic carbon related bands located at *ca.*1350 cm^{-1} (D band) and 1590 cm^{-1} (G band), with the I_D/I_G values of 0.97 and 0.91 for 3DG and GQD/3DG, respectively, implying some of the defects of the 3DG were removed during the deposition of GQDs. Importantly, the similarities in XRD and Raman profiles of the 3DG and the GQD/3DG composite confirm that the electrodeposition of GQDs was benign enough to anchor the GQDs on the 3DG surface without damaging the original 3D structure. Meanwhile, as shown in Fig. 3c, the conductivity of the GQD/3DG-10h was measured to be 3.7 S m^{-1}, nearly 10 times more than that of the 3DG (0.35 S m^{-1}). As conductivity is an important parameter for the supercapacitor electrode materials, such a notable improvement in the conductivity induced by the deposition of GQDs would reduce the series resistance and facilitate charge transport in the assembled supercapacitor, potentially leading to a supercapacitor with much better performance.

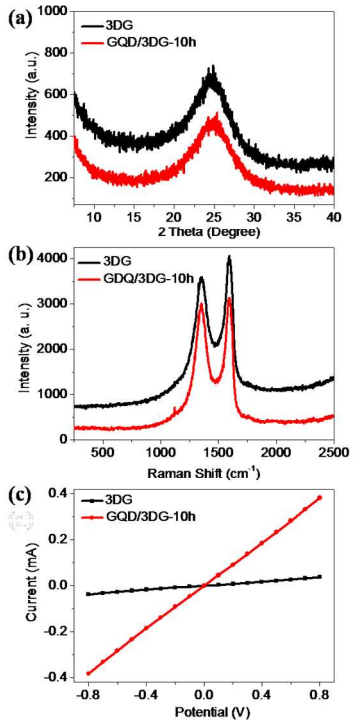

Fig. 3. (a) XRD spectra and (b) Raman profiles of the 3DG and GQD/3DG-10h composite. (c) Room temperature *I-V* characteristics of the 3DG and GQD/3DG-10h composite exhibiting ohmic characteristics.

Despite of the resemblance in XRD and Raman profiles, the 3DG and GQD/3DG obviously differed in the specific surface area and pore size distributions measured by the isotherms of N_2 adsorption-desorption. The nitrogen cryo-adsorption isotherms are shown in Fig. 4a, where both 3DG and GQD/3DG composites show a Type IV isotherm characteristics with a wide hysteresis loop indicating the existence of mesopores. Pore size distribution curves in Fig. 4b reveal a narrow distribution of pores with diameters ranging from 1 to 5 nm, the presence of micropores with a diameter less than 2 nm is significantly increased after the GQD deposition, presumably due to the formation of new interstices between deposited GQDs and/or the 3DG scaffold. As a result, the Brunauer-Emmett-Teller (BET) surface area of GQD/3DG composites with 5 h and 10 h GQD deposition is 216 and 292 m^2 g^{-1}, respectively, which is significantly higher than that of the pristine 3DG (192 m^2 g^{-1}), therefore rendering a much larger electrode/electrolyte interface that would contribute to the EDL capacitance found in the supercapacitor.

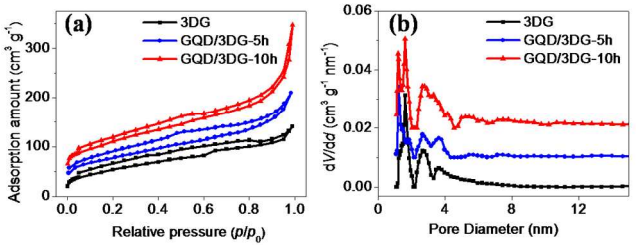

Fig. 4. N_2 adsorption-desorption isotherms (a) and pore size distributions (b) of

the 3DG, GQD/3DG-5h and GQD/3DG-10h composites, respectively.

Electrochemical properties

Symmetrical two-electrode supercapacitors were fabricated by separating two identical films of either the pristine 3DG (Device A) or the GQD/3DG composites with different GQD deposited time of 5 h (Device B) and 10 h (Device C), with a piece of filter paper fully soaked in 1 M H_2SO_4 solution as the electrode separator. Their electrochemical performances were evaluated by CV and galvanostatic charge/discharge tests in the potential range of 0 to 0.8 V. The 3DG is known to be a promising material for supercapacitors, and as plotted in Fig. 5a, Device A showed typical capacitive CV curves close to ideal electrochemical double layer behavior. Upon the deposition of GQDs on the surface of 3DG, the CV curves of Devices B and C remained undistorted in both anodic and cathodic directions even at high scan rates (Fig. 5b and 5c), implying that electrodepositing GQDs did not have any adverse effect on the EDL at the electrode/electrolyte interface. Meanwhile, the capacitive current of Devices B and C notably increased at all scan rates after the anchorage of GQDs on the 3DG, suggesting that the deposition of the GQDs well improved the electrochemical capacitance of the composite electrode. Compared to the 3DG, the GQD/3DG composites had a larger specific surface area to render more surface active sites and accessible edges for the ion adsorption/desorption, therefore improving the EDL capacitive properties of the electrode.[31] It is interesting to note that the area surrounded by the CV curves for Devices A to C increases in the following order of A < B < C, implying Device C would have the highest specific capacitance as the specific capacitance of the supercapacitor was reported to be directly related to the area surrounded by the CV curves measured at the same scan rate.[38]

As shown in Fig. 5d to f, the specific capacitances of the Devices A to C were further measured by a galvanostatic charge–discharge experiment between 0 and +0.8 V at different discharge currents. No obvious IR drop was observed on the start of all discharge curves, indicating that all the devices had a small internal series resistance and efficient extraction of stored energy, as was also confirmed by the linear and symmetrical charge-discharge curves. The mass-specific capacitance C_m is calculated from the equation: $C_m = 2I/m(dV/dt)$,[39] where I is the discharge current, dV/dt is the slope of the discharge curve and m is the mass of one electrode, respectively. The calculated specific capacitance are 136 F g^{-1} , 192 F g^{-1} and 268 F g^{-1} at a discharge current density of 1.25 A g^{-1} (I = 125 μA) for Devices A, B and C, respectively. In agreement with the CV curves in Fig. 5a to c, the specific capacitances of Device B and C are larger than Device A, suggesting the effectiveness of depositing GQDs in improving the performance of 3DG supercapacitors. An optimized GQDs deposition time of 10 h renders the best device, Device C, with a high capacitance of 268 F g^{-1}, which is among the best values reported for supercapacitors based on 3D graphene or graphene/metal oxide composites (Table 1).

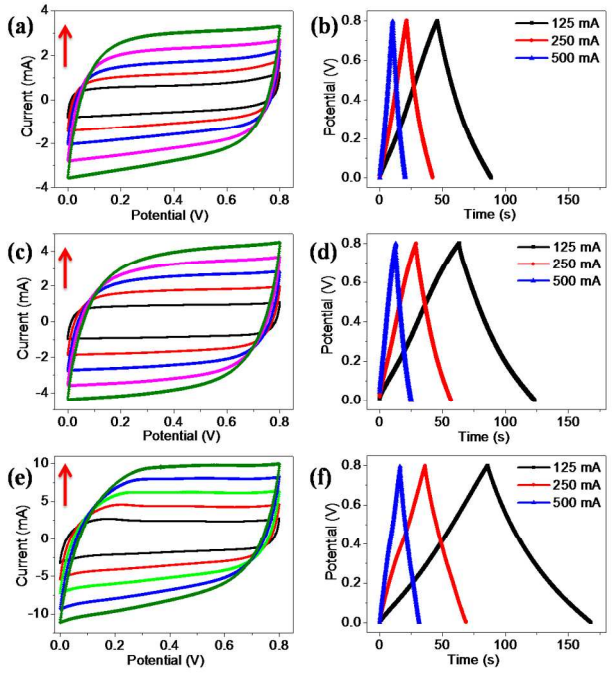

Fig. 5. (a) to (c) are CV curves of supercapacitors based on the 3DG (Device A) and GQD/3DG composites with 5 h (Device B) and 10 h (Device C), respectively. Scan rates are 0.2 V s^{-1}, 0.4 V s^{-1}, 0.6 V s^{-1}, 0.8 V s^{-1} and 1 V s^{-1}, respectively, and the arrows indicate the direction of increasing scan rates. (d) to (f) are galvanostatic charge-discharge curves at different discharge currents for Devices A, B and C, respectively.

Table 1 Direct comparison of the specific capacitance (C_m) of supercapacitors based on different 3DG materials.

No.	Electrode materials	C_m (F g^{-1})	Ref
1	$Ni(OH)_2$/graphene and porous graphene	218.4	10
2	3D graphene aerogel	128	40
3	MnO_2 deposited on graphene oxide composites	216	8
4	N-Doped graphitic carbon nanocages	248	41
5	3D Graphene hydrogel Films	186	42
6	Silver nanoparticles decorated graphene foam	110	43
7	Mn_3O_4/reduced graphene oxide hydrogel	148	44
8	Composite of Mn_2O_3 with 3D graphene/CNTs	280	45
9	N-doped graphene–CNT networks	180	46
10	3D MnO_2/graphene hydrogel	242	47
11	Composite of graphene and activated carbon	116.5	14
12	GQD/3DG-10h composite	268	Current

To rule out any possibility that the GQD deposition process could contribute to the performance improvement in the supercapacitor, control samples of 3DG was immersed in a *GQD-free* solution and subjected to a +2 V bias for 10 h before they were eventually assembled in the same symmetrical two-electrode configuration to give Device D. Fig. S1 shows the galvanostatic charge-discharge curves of Device D at a current density of 1.25 A g^{-1}, 2.5 A g^{-1} and 5 A g^{-1}, respectively. The calculated capacitance from the charge-discharge curve is 131 F g^{-1} at a discharge current density of 1.25 A g^{-1}, matching that of the Device A (3DG) and confirming that the observed notable

improvement in the supercapacitor performance is related to the deposition of GQDs rather than the application of the bias in the electrodeposition process.

Electrochemical impedance spectroscopy (EIS) was performed to further evaluate the electrochemical performance of Devices A and C. For an ideal EDLC, the low frequency region of its Nyquist plot is a straight line perpendicular to real axis of the impedance. Fig. 6a compares the EIS spectra of both devices, where both curves are close to the imaginary axis at low frequencies and show characteristics approaching the ideal EDLC. However, the EIS spectrum of Device C (red curve) was more vertical to real axis than that of Device A, revealing a more ideal capacitive behavior of Device C than Device A.[48,49] The lack of an obvious RC semicircle at high frequencies in both devices indicates the fast charge transfer across the electrode/electrolyte interface in both 3DG and GQD/3DG composite materials that leads to the excellent conditions of the assembled supercapacitors.

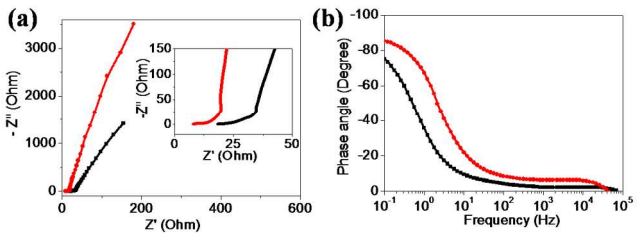

Fig. 6. (a) Nyquist plots of Devices A (black) and C (red) measured at open-circuit conditions. The inset shows the enlarged area with impedance values between 0 and 50 Ω. (b) Bode plots of Devices A and C.

Meanwhile, the high-frequency intercept with the real axis is the equivalent series resistance (R_s), representing the sum of the electrolyte solution resistance, the intrinsic resistance of active material and the contact resistance at the electrode/electrolyte interface.[50] From the magnified high-frequency region in the inset of Fig. 6a, it is clearly observed that the Device C has a lower R_s value than that of Device A, showing the deposition of GQDs helped to decreased the undesired R_s and contributed to the improved performance for the GQD/3DG supercapacitor.[51] The dependence of phase angle on the frequency of the supercapacitors is plotted in Fig. 6b. In the Bode plot, an ideal EDLC would have a phase angle close to 90° at low frequencies. Herein, the phase angles of the Device A and Device C are 83.8° and 87.3° at 0.01 Hz, respectively. More importantly, the phase angle of Device C is higher than 80° at any frequency lower than 1Hz, implying that compared to Device A, Device C approaches an ideal EDLC and the deposition of GQDs effectively improved the capacitive property of the 3DG supercapacitor.[36] It is reported that the capacitive behavior of EDLCs could be classified in two different categories in view of the pore size of the electrode material, where mesoporous carbons of pores larger than 2 nm are governed by the traditional double layer model and carbon materials of micropores commensurate with 1 nm or less are well described by an electric double-cylinder capacitor (EDCC) model associated with the curvature effect of the electrode surface.[4,52] Since the size of the GQDs is only 2–5 nm, it is probable that subnanometer pores were created between deposited GQDs and the 3DG scaffold or even between neighboring GQDs, aligning partially or completely desolvated electrolyte ions in these cylindrical pores and forming the "electric wire in cylinder".[4] This is well supported by the notably increased presence of ~1 nm and subnanometer pores with the deposition of GQDs shown in Fig. 4b, and consequently, the supercapacitor based on the GQD/3DG electrodes can be better described as a combination of EDLC and EDCC, a phenomenon also observed by Hahm et al in a supercapacitor constructed on a carbon nanotube/nanocup hybrid structure.[53]

The cycling stability of the supercapacitor is an important parameter to evaluate its potential for practical applications. Fig. 7 summarizes the temporal evolution of the specific capacitance of Device C over consecutive charge-discharge cycles at a current density of 5 A g^{-1}. The device retained more than 90% of its initial capacitance after 5,000 charge-discharge cycles and no obvious degradation in the capacitance could be observed during the cycling experiment, indicating that our GQD/3DG supercapacitor has a good long-term electrochemical stability.

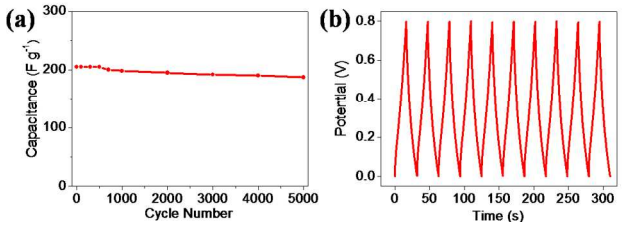

Fig. 7. (a) The capacitance of Device C under the cycling tests for 5000 charge-discharge cycles and (b) the process of ten charge-discharge cycles.

Conclusions

In summary, we have successfully demonstrated an electrochemical deposition method to assemble the GQD on the 3DG electrodes and tested their performance as supercapacitors. The electrochemical assembly of the GQD on the 3DG proceeded smoothly and led to the formation of a uniform film on the surface of the 3DG. Supercapacitors fabricated from GQD/3DG composite electrodes with 10 h GQD deposition exhibited a high capacitance of 268 F g^{-1}, representing a more than 90% improvement over that of bare 3DG electrodes (136 F g^{-1}). Considering the convenience of the electrodeposition of GQDs, the current method could also be used in other well-defined electrode materials, such as carbon nanotubes, carbon aerogels and so on, to further boost the performance of the supercapacitors.

Notes and references

[a] *Key Laboratory of Cluster Science, Ministry of Education of China; Beijing Key Laboratory of Photoelectronic/Electrophotonic Conversion Materials;*
School of Chemistry, Beijing Institute of Technology, Beijing 100081, China; E-mail: Zhipan@bit.edu.cn;lqu@bit.edu.cn (L. Qu)
‡ *These authors contributed equally to this work.*
† Electronic Supplementary Information (ESI) available: [details of any supplementary information available should be included here]. See DOI: 10.1039/b000000x/

‡ Footnotes should appear here. These might include comments relevant to but not central to the matter under discussion, limited experimental and spectral data, and crystallographic data.

1 W. Lu, L.T. Qu, K. Henry and L.M. Dai, *J. Power Sources*, 2009, **189**, 1270.
2 Z. Chen, D. Wang, X.L. Wang, Y.H. Cheng, G. Wang and Y.F. Lu, *Chem. Commun.*, 2012, **48**, 3736.
3 Z.L. Wang and J.H. Song, *Science*, 2006, **312**, 242.
4 P. Simon and Y. Gogotsi, *Nat. Mater.*, 2008, **7**, 845.
5 W. Chen, R.B. Rakhi, L.B. Hu, X. Xie, Y. Cui and H.N. Alshareef, *Nano Lett.*, 2011, **11**, 5165.
6 B.E. Conway, V. Birss and J. Wojtowicz, *J. Power Sources*, 1997, **66**, 1.
7 Z.S. Wu, D.W. Wang, W. Ren, J. Zhao, G. Zhou, F. Li and H.M. Cheng, *Adv. Funct. Mater.*, 2010, **20**, 3595.
8 C.Z. Yuan, L. Yang, L.R. Hou, L.F. Shen, X.G. Zhang and X.W. Lou, *Energy Environ. Sci.*, 2012, **5**, 7883.
9 S. Chen, J.W. Zhu, X.D. Wu, Q.F. Han and X. Wang, *ACS Nano*, 2010, **4**, 2822.
10 G.H. Yu, L.B. Hu, N.A. Liu, H.L. Wang, M. Vosgueritchian, Y. Yang, Y. Cui and Z.A. Bao, *Nano Lett.*, 2011, **11**, 4438.
11 J. Yan, Z.J. Fan, W. Sun, G.Q. Ning, T. Wei, Q. Zhang, R.F. Zhang, L.J. Zhi and F. Wei, *Adv. Funct. Mater.*, 2012, **22**, 2632.
12 T.C. Girija and M.V. Sangaranarayanan, *J. Power Sources*, 2006, **156**, 705.
13 Q.Q. Zhou, J. Gao, C. Li, J. Chen and G.Q. Shi, *J. Mater. Chem. A*, 2013, **1**, 9196.
14 Z.L. Dong, C.C. Jiang, H.H. Cheng, Y. Zhao, G.Q. Shi, L. Jiang and L.T. Qu, *Adv. Mater.*, 2012, **24**, 1856.
15 K.S. Novoselov, A.K. Geim, S.V. Morozov, D. Jiang, Y. Zhang, S.V. Dubonos, I. V. Grigorieva and A.A. Firsov, *Science*, 2004, **306**, 666.
16 K.S. Novoselov, A.K. Geim, S.V. Morozov, D. Jiang, M.I. Katsnelson, I.V. Grigorieva, S.V. Dubonos and A.A. Firsov, *Nature*, 2005, **438**, 197.
17 Y. Zhang, Y.W. Tan, H.L. Stormer and P. Kim, *Nature*, 2005, **438**, 201.
18 K.W. Chen, L.B. Chen, Y.Q. Chen, H. Bai and L. Li, *J. Mater. Chem.*, 2012, **22**, 20968.
19 T.Y. Kim, G. Jung, S. Yoo, K.S. Suh and R.S. Ruoff, *ACS Nano*, 2013, **7**, 6899.
20 Y. Zhao, C.G. Hu, Y. Hu, H.H. Cheng, G.Q. Shi and L.T. Qu, *Angew. Chem. Int. Ed.*, 2012, **51**, 11371.
21 L. Zhang and G.Q. Shi, *J. Phys. Chem. C*, 2011, **115**, 17206.
22 C.G. Hu, H.H. Cheng, Y. Zhao, Y. Hu, Y. Liu, L.M. Dai and L.T. Qu, *Adv. Mater.*, 2012, **24**, 5493.
23 Y.X. Xu, K.X. Sheng, C. Li and G.Q. Shi, *ACS Nano*, 2010, **4**, 4324.
24 Y. Li, Y. Zhao, H.H. Cheng, Y. Hu, G.Q. Shi, L.M. Dai and L.T. Qu, *J. Am. Chem. Soc.*, 2012, **134**, 15.
25 Z.P. Zhang, J. Zhang, N. Chen and L.T. Qu, *Energy Environ. Sci.*, 2012, **5**, 8869.
26 J.H. Shen, Y.H. Zhu, X.L. Yang and C.Z. Li, *Chem. Commun.*, 2012, **48**, 3686.
27 S.J. Zhu, J.H. Zhang, C.Y. Qiao, S.J. Tang, Y.F. Li, W.J. Yuan, B. Li, L. Tian, F. Liu, R. Hu, H.N. Gao, H.T. Wei, H. Zhang, H.C. Sun and B. Yang, *Chem. Commun.*, 2011, **47**, 6858.
28 H. Razmi and R. Mohammad-Rezaei, *Biosens. Bioelectron.*, 2013, **41**, 498.
29 Y. Li, Y. Hu, Y. Zhao, G.Q. Shi, L.E. Deng, Y.B. Hou and L.T. Qu, *Adv. Mater.*, 2011, **23**, 776.
30 L. Tang, R. Ji, X. Cao, J. Lin, H. Jiang, X. Li, K.S. Teng, C.M. Luk, S. Zeng, J. Hao and S.P. Lau, *ACS Nano*, 2012, **6**, 5102.
31 W.W. Liu, Y.Q. Feng, X.B. Yan, J.T. Chen and Q.J. Xue, *Adv. Funct. Mater.*, 2013, **23**, 4111.
32 Y.R. Zhu, X.B. JI, C.C. Pan, Q.Q. Sun, W.X. Song, L.B. Fang, Q.Y. Chen and C.E. Banks, *Energy Environ. Sci.*, 2013, **6**, 3665.
33 Y. Hu, Y. Zhao, G.W. Lu, N. Chen, Z. P. Zhang, H. Li, H.B. Shao and L.T. Qu, *Nanotechnology*, 2013, **24**, 195401.
34 H.C. Schniepp, J.L. Li, M.J. McAllister, H. Sai, M. Herrera-Alonso, D.H. Adamson, R.K. Prud'homme, R.K. Car, D.A. Saville and I.A. Aksay, *J. Phys. Chem. B*, 2006, **110**, 8535.
35 Y. Liu, C.Y. Liu and Z.Y. Zhang, *J. Colloid Interf. Sci.*, 2011, **356**, 416.
36 L.B. Zhang, G.Y. Chen, M.N. Hedhili, H.N. Zhang and P. Wang, Nanoscale, 2012, **4**, 7038.
37 Y.X. Xu, K.X. Sheng, C. Li and G.Q. Shi, *ACS Nano*, 2010, **4**, 4324.
38 X.R. Wen, D.S. Zhang, L.Y. Shi, T.T. Yan, H. Wang and J.P. Zhang, *J. Mater. Chem.*, 2012, **22**, 23835.
39 Y.N. Meng, Y. Zhao, C.G. Hu, H.H. Cheng, Y. Hu, Z.P. Zhang, G.Q. Shi and L.T. Qu, *Adv. Mater.*, 2013, **25**, 2326.
40 X.T. Zhang, Z.Y. Sui, B. Xu, S.F. Yue, Y.J. Luo, W.C. Zhan and B. Liu, *J. Mater. Chem.*, 2011, **21**, 6494.
41 Y.M. Tan, C.F. Xu, G.X. Chen, Z.H. Liu, M. Ma, Q.J. Xie, N.F. Zheng and S.Z. Yao, *ACS Appl. Mater. Interfaces*, 2013, **5**, 2241.
42 Y.X. Xu, Z.Y. Lin, X.Q. Huang, Y. Liu, Y. Huang and X.F. Duan, *ACS Nano*, 2013, **5**, 4042.
43 A. Bello, M. Fabiane, D. Dodoo-Arhin, K. I. Ozoemena and N. Manyala, *J. Phys. Chem. Sol.*, 2014, **1**, 109.
44 L. Li, Z.A. Hu, Y.Y. Yang, P.J. Liang, A.L. Lu, H. Xu, Y.Y. Hu and H.Y. Wu, *Chin. J. Chem.*, 2013, **10**, 1290.
45 Y.F. Zhang, M.Z. Ma, Y. Jun, H. Wei and X.C. Dong, *RSC Adv.*, 2014, **4**, 8466.
46 B. You, L.L. Wang, L. Yao and J. Yang, *Chem. Commun.*, 2013, **49**, 5016.
47 S.S. Wu, W.F. Chen and L.F. Yan, *J. Mater. Chem. A*, 2014, **2**, 2765.
48 M.D. Stoller, S.J. Park, Y.W. Zhu, J.H. An and R.S. Ruoff, *Nano Lett.*, 2008, **8**, 3498.
49 W.W. Liu, X.B. Yan, J.T. Chen, Y.Q. Feng and Q.J. Xue, *Nanoscale*, 2013, **5**, 6053.
50 H.M. Sun, L.Y. Cao and L.H. Lu, *Energy Environ. Sci.*, 2012, **5**, 6206.
51 A. Celzard, F. Collas, J.F. Mareche, G. Furdin and I. Rey, *J. Power Sources*, 2002, **108**, 153.
52 J.S. Huang, B.G. Sumpter and V. Meunier, *Angew. Chem. Int. Ed.*, 2008, **47**, 520.
53 M. G. Hahm, A.L.M. Reddy, D.P. Cole, M. Rivera, J.A. Vento, J. Nam, H.Y. Jung, Y.L. Kim, N.T. Narayanan, D.P. Hashim, C. Galande, Y.J. Jung, M. Bundy, S. Karna, P.M. Ajayan and R. Vajtai, *Nano Lett.*, 2012, **12**, 5616.